

Constraining compact star properties with nuclear saturation parameters

Jia Jie Li^{1,*} and Armen Sedrakian^{2,3,†}

¹*Institute for Theoretical Physics, J. W. Goethe University, D-60438 Frankfurt am Main, Germany*

²*Frankfurt Institute for Advanced Studies, D-60438 Frankfurt am Main, Germany*

³*Institute of Theoretical Physics, University of Wrocław, 50-204 Wrocław, Poland*

(Dated: January 7, 2022)

A set of nuclear equation of states (EoS) derived from density-dependent relativistic density functional theory and constrained by terrestrial experiments, astrophysical observations, in particular by the GW170817 event, and chiral effective field (χ EFT) theory of neutron matter is used to obtain a generic EoS parameterized in terms of a few characteristics defined at the saturation. We explore the sensitivity of the resulting generic parametrization of the EoS and find that the gross properties of compact stars are most sensitive to the isoscalar skewness coefficient Q_{sat} (quantifying the density-expansion at third order) and the isovector slope coefficient L_{sym} (quantifying the isospin-expansion at the second order) around saturation density. More specifically, (i) among these Q_{sat} is the dominant parameter controlling both the maximum mass and the radius of a compact star while L_{sym} is constrained by χ EFT of neutron matter; (ii) massive enough ($M \sim 2 M_{\odot}$) compact stars featuring both hyperons and Δ 's can be obtained if the value of Q_{sat} is large enough; (iii) the emergence of Δ 's reduces the radius of a canonical mass ($M \sim 1.4 M_{\odot}$) compact star thus easing the tension between the predictions of the relativistic density functionals and the inferences from the X-ray observation of nearby isolated neutron stars.

I. INTRODUCTION

Compact stars are unique laboratories for studies of dense matter. The hadronic core of a compact star extends from half up to a few times the nuclear saturation density ρ_{sat} . Currently, the most rigorous constraint on the high-density behavior of the equation of state (EoS) comes from the observations of a few massive pulsars with masses $\sim 2 M_{\odot}$ [1–3]. These observations set a lower bound on the maximum mass predicted by any EoS of dense baryonic matter. The recent detection of gravitational waves from the binary neutron star inspiral event GW170817 [4] allowed to place constraints on the tidal deformability of compact stars and thus to put additional constraints on the EoS [5–11]. The GW170817 event is complementary to the mass measurements indicated above as it allows one to put constraints on the properties (specifically, radius and deformability) of a canonical-mass ($M \sim 1.4 M_{\odot}$) neutron star.

The details of the composition of compact stars at high densities are not fully understood yet and the possibilities include hyperonization [12–23], appearance of Δ resonances [12, 24–27] and transition from hadronic to quark matter [28–35]; for recent reviews see [36–39].

Observational information on masses and radii does not resolve the underlying composition of matter. In particular, the Bayesian inferences [40–43] of these parameters from the data infer only the total pressure as a function of density. However, many phenomena associated with neutron stars, e.g., their cooling, depend in an essential way on the composition of matter in the entire range from the crust to the core of the star. Their modelling requires as an input microscopically derived EoS or parametrizations thereof - a problem that we will address in this work. The current observational programs

focusing on neutron stars combined with the nuclear physics modeling of their interiors are aimed at unraveling the features of the matter compressed to very high densities.

Among various possibilities mentioned just above, the hyperonization of dense matter becomes a serious possibility because hyperons are energetically favored as the density increases inside a neutron star; for recent reviews see Refs. [36, 37, 39]. The onset of hyperons entails a considerable softening of the EoS and thus reduces the maximum mass of corresponding sequences of compact stars compared to those based on purely nucleonic EoS [16–22]. The existence of new degrees of freedom in the core of a neutron star cannot be confirmed or ruled out so far on the basis of astrophysical observations alone.

The physics of nuclear systems at and somewhat below the saturation and zero temperature is well constrained by the studies of finite nuclei. The EoS of isospin symmetrical nuclear matter around saturation density is well constrained, because physical observables that are dominated by the isoscalar sector have been measured with very high precision. On the other hand, the isovector sector remains poorly determined as the measurements of the observables that are sensitive to the isovector channel lack the necessary precision. Pure neutron matter sets the limiting behaviour of isovector properties of nuclear matter. In particular, the neutron matter EoS, obtained by solving the many-body Hamiltonian derived from chiral effective field theory (χ EFT), is expected to be reliable up to densities $\sim 1.3\rho_{\text{sat}}$ [44]. This allows one to gauge the phenomenological theories of isospin asymmetrical matter by requiring that in the limit of pure neutron matter the *ab-initio* results for the EoS are reproduced.

Clearly, any viable EoS must simultaneously satisfy the constraints from experimental and theoretical studies of nuclear systems near the saturation density and the observational constraints deduced from studies of compact stars. In this work we present a density functional based generic parametrization of the dense matter EoS for the hadronic matter that (i) reproduces the saturation properties of isospin-

* jjiali@itp.uni-frankfurt.de

† sedrakian@fias.uni-frankfurt.de

symmetric nuclear matter; (ii) in the limit of pure neutron matter matches the χ EFT-based *ab initio* results for the EoS of neutron matter, (iii) produces compact star sequences with $M_{\text{max}} \gtrsim 2 M_\odot$ and $R_{M_{1.4}} = 11.8 - 13.8$ km, where $R_{M_{1.4}}$ is the radius of $1.4 M_\odot$ mass star; (iv) allows for strangeness in the form of hyperons as well as for Δ resonances. The key new feature of our study is the mapping of the density-functional based EoS onto a generic one that is parametrized in terms of a few observables of nuclear systems at saturation, which we call *characteristic parameters or characteristics*, see Eq. (9) below.

Similar explorations were previously carried out using Skyrme density functionals in order to constrain the symmetry energy by evaluating the neutron skin [45, 46], giant monopole resonances [47], and the electric dipole polarizability [48]. Correlations between the critical density of Δ resonance formation and the maximum mass of neutron stars within the nonlinear (NL) density functional theory has also been studied in Refs. [49, 50]. Furthermore, the tidal polarizability of a neutron star has been applied to constrain the symmetry energy within the NL-density functional theory [51]. Also, nucleonic EoS based on the Taylor expansions around the saturation density has been applied to assess the effect of the high-order characteristics [52, 53] as well as to put potential constraints among them [53].

The paper is organized as follows. In Sec. II we outline the framework necessary to compute the stellar structure and the general properties of asymmetric nuclear matter. In Sec. III we show how the uncertainties in the values of nuclear matter characteristics at the saturation influence the parameters of the compact stars. This is combined with the constraints on the available parameter space set by the current theoretical and observational information. Finally, Sec. IV summarizes our concluding remarks.

II. THEORETICAL FRAMEWORK

A. EoS of hadronic matter

We use here the standard form of the Hartree density functional in which Dirac baryons are coupled via meson fields [54, 55]. The theory is Lorentz invariant and, therefore, preserves causality when applied to high-density matter. The baryon octet interacts via exchanges of σ , ω and ρ mesons, which comprise the minimal set necessary for a quantitative description of nuclear phenomena [56]. In addition we consider two hidden-strangeness mesons (σ^* , ϕ) which describe interactions between hyperons [14, 21, 23].

The Lagrangian is given by the sum of the free baryonic and mesonic Lagrangians, which we do not write down, and the interaction Lagrangian which reads

$$\mathcal{L}_{\text{int}} = \sum_B \bar{\psi}_B \left(-g_{\sigma B} \sigma - g_{\sigma^* B} \sigma^* - g_{\omega B} \gamma^\mu \omega_\mu - g_{\phi B} \gamma^\mu \phi_\mu - g_{\rho B} \gamma^\mu \vec{\rho}_\mu \cdot \vec{\tau}_B \right) \psi_B + \sum_D (\psi_B \rightarrow \psi_D^*), \quad (1)$$

where ψ stands for the Dirac spinor and ψ^ν for the Rarita-Schwinger spinor. The index B labels the spin-1/2 baryonic octet, which comprises nucleons $N \in \{n, p\}$, and hyperons $Y \in \{\Lambda, \Xi^{0,-}, \Sigma^{+,0,-}\}$. The index D refers to the spin-3/2 resonance quartet of Δ 's ($\Delta \in \{\Delta^{++}, \Delta^{+}, \Delta^0, \Delta^{-}\}$) which are treated as Rarita-Schwinger particles [57]. The mesons couple to the baryons and Δ 's with the strengths determined by the coupling constants g_{mB} and g_{mD} , which are functionals of the vector density. The Lagrangian (1) is minimal, as it does not contain (a) isovector-scalar δ meson [58] and (b) the π meson and the tensor couplings of vector meson to baryons, both of which arise in the Hartree-Fock theories [59, 60], which are beyond the scope of this paper.

In the nucleonic sector, the meson-nucleon (mN) couplings are given by [61, 62]

$$g_{mN}(\rho_v) = g_{mN}(\rho_{\text{sat}}) f_{mN}(r), \quad (2)$$

where $r = \rho_v / \rho_{\text{sat}}$ and ρ_v is the baryon vector density. For the isoscalar channel, one has

$$f_{mN}(r) = a_m \frac{1 + b_m(r + d_m)^2}{1 + c_m(r + d_m)^2}, \quad m = \sigma, \omega, \quad (3)$$

with $f_{mN}(1) = 1$, $f_{mN}''(0) = 0$ and $f_{mN}''(1) = f_{mN}''(1)$. The density dependence for the isovector channel is taken in an exponential form

$$f_{mN}(r) = e^{-a_m(r-1)}, \quad m = \rho. \quad (4)$$

It is seen that if we take the baryon and meson masses to be (or close to) the ones in the vacuum, then the Lagrangian is fixed and, therefore, the properties of infinite nuclear matter can be computed uniquely in terms of seven adjustable parameters. These are the three coupling constants at saturation density ($g_{\sigma N}$, $g_{\omega N}$, $g_{\rho N}$), and four parameters (a_σ , b_σ , a_ω , a_ρ) that control their density dependence.

The vector mesonhyperon couplings (mY) are given by the SU(6) spin-flavor symmetric quark model [17, 19, 21, 60] whereas the scalar mesonhyperon couplings are determined by fitting to certain preselected properties of hypernuclear systems. We determine the coupling constants, $g_{\sigma Y}$, using the following hyperon potentials in the symmetric nuclear matter at ρ_{sat} [63, 64]:

$$U_\Lambda^{(N)} = -U_\Sigma^{(N)} = -30 \text{ MeV}, \quad U_\Xi^{(N)} = -14 \text{ MeV}. \quad (5)$$

Physically, the $\Lambda\Lambda$ bond energy provides a rough estimate of the $U_\Lambda^{(\Lambda)}$ potential at the average Λ density ($\approx \rho_{\text{sat}}/5$) inside a hypernucleus [16]. We adopt the value

$$U_\Lambda^{(\Lambda)}(\rho_{\text{sat}}/5) = -0.67 \text{ MeV}, \quad (6)$$

which reproduces the most accurate experimental value to date [65]. This information we use to fix the value of the coupling $g_{\sigma^* \Lambda}$. The coupling of remaining hyperons Ξ and Σ to the σ^* is constrained by the relations $g_{\sigma^* Y} / g_{\phi Y} = g_{\sigma^* \Lambda} / g_{\phi \Lambda}$. More detailed discussions regarding hyperon potentials can be found, for instance, in Refs. [22, 60, 66].

TABLE I. The characteristic parameters of symmetric nuclear matter at saturation density for DD-ME2 parametrization [77]. The bold parameters are those that can be calibrated by the density functional alone. The definitions of parameters are as in Ref. [78]. The ρ_{sat} is in unit of fm^{-3} , M_D^* in nucleon mass, and the rest are in units of MeV.

		Isoscalar characteristics			
ρ_{sat}	M_D^*	E_{sat}	K_{sat}	Q_{sat}	Z_{sat}
0.152	0.57	-16.14	251.15	479	4448
		Isovector characteristics			
		E_{sym}	L_{sym}	K_{sym}	Q_{sym}
		32.31	51.27	-87	777

The isoscalar meson- Δ couplings are uncertain, as no consensus has been reached yet on the magnitude of the Δ potential in nuclear matter. The studies of the scattering of electrons and pions off nuclei and photoabsorption which are based on a phenomenological models [67, 68] indicate that the Δ isoscalar potential V_Δ should be in the range [69]

$$-30 \text{ MeV} + V_N(\rho_{\text{sat}}) \lesssim V_\Delta(\rho_{\text{sat}}) \lesssim V_N(\rho_{\text{sat}}), \quad (7)$$

where V_N is the nucleon isoscalar potential. The studies of Δ production in heavy-ion collisions [70, 71] suggest a less attractive potential [72],

$$V_N(\rho_{\text{sat}}) \lesssim V_\Delta(\rho_{\text{sat}}) \lesssim 2/3 V_N(\rho_{\text{sat}}). \quad (8)$$

At the same time, the isovector meson- Δ couplings are largely unknown. Below, we limit ourselves to the case where $R_{\Delta\omega} = g_{\omega\Delta}/g_{\omega N} = 1.1$, $g_{\rho\Delta}/g_{\rho N} = 1.0$ and $g_{\sigma\Delta}$ is determined by fitting to the Δ -potential at saturation density ρ_{sat} . The value $R_{\Delta\omega} = 1.1$ allows one to obtain a physical solution for very attractive Δ -potentials [27]. Notice that the density dependence of the meson- $Y(\Delta)$ couplings are the same as the meson-nucleon ones.

Once the coupling constants are determined, one could compute the EoS of stellar matter by implementing the additional conditions of weak equilibrium and charge neutrality that prevail in neutron stars. We further match smoothly our EoS for the core to that of the crust EoS given in Refs. [73, 74] at the crust-core transition density $\rho_{\text{sat}}/2$. The integral parameters of a compact star, in particular, the mass and the radius, are then computed from the Tolman-Oppenheimer-Volkoff (TOV) equations [75, 76].

B. Characteristic parameters of nuclear matter

As is well known, the EoS of isospin asymmetric nuclear matter can be expanded close to the saturation and the isospin symmetrical limit in power series

$$E(\rho, \delta) \simeq E_{\text{sat}} + \frac{1}{2!} K_{\text{sat}} n^2 + \frac{1}{3!} Q_{\text{sat}} n^3 + E_{\text{sym}}(\rho) \delta^2 + L_{\text{sym}}(\rho) \delta^2 n + O(n^4, n^2 \delta^2), \quad (9)$$

where $n = (\rho - \rho_{\text{sat}})/3\rho_{\text{sat}}$ and $\delta = (\rho_n - \rho_p)/\rho$. The coefficients of the density-expansion given by the first line of Eq. (9) are

known as the empirical parameters of nuclear matter in the isoscalar channel, specifically, the saturation energy E_{sat} , the incompressibility K_{sat} , and the skewness Q_{sat} . The isovector characteristics associated with the expansion away from the symmetrical limit [the second line in Eq. (9)] are the symmetry energy parameter E_{sym} and its slope parameter L_{sym} . The explicit expressions for the above parameters, as well as the higher-order terms not shown here can be found, for instance, in Refs. [53, 78].

The expansion above assumes that δ and n are sufficiently small and are of the same order of magnitude (note that δ appears in even powers only). It is then seen that the various characteristics of the bulk nuclear matter are classified simply according to the order at which they contribute to the energy density. The binding energy as a function of density and isospin asymmetry alone does not allow us to determine all the parameters of both the isoscalar-scalar and -vector channels of a relativistic density functional. In addition, one needs to specify the value of the Dirac mass M_D^* at the saturation which is crucial for a quantitative description of finite nuclei, e.g., spin-orbit splitting.

Given the five macroscopic characteristics in Eq. (9) together with the preassigned values of ρ_{sat} and M_D^* , we are in a position to determine uniquely the seven adjustable parameters of the density functional defined above. Having this in mind, our strategy would be to vary individually these macroscopic characteristics within their acceptable ranges and to examine transparently the influence of these variations on the nuclear matter properties. In this manner, we explore the correlation(s) between any given property of nuclear matter and/or compact stars and each parameter entering Eq. (9). Of particular interest are the quantities which arise at a higher order of the expansion, specifically, Q_{sat} and L_{sym} . Their values are weakly constrained by the conventional fitting protocol used in constructing the density functionals, i.e., the procedure which involves usually fits to nuclear masses, charge radii and neutron skins.

As a reference for the correlation analyses below, we adopt the DD-ME2 parameter set [77]. This parametrization has been tested on the entire nuclear chart with great success. It also agrees with experimental knowledge about the empirical parameters of nuclear matter. In Table I we list the characteristic parameters of symmetric nuclear matter at saturation according to the DD-ME2 parametrization.

III. RESULTS AND DISCUSSIONS

A. Low-density neutron matter

As outlined in the previous section, the nuclear matter EoS close to the saturation can be characterized in terms of double-expansion around the saturation density and isospin-symmetrical limit. The coefficients of the expansion can be considered as *characteristic parameters (or characteristics)* of nuclear matter, whereby the low-order parameters E_{sat} , K_{sat} , E_{sym} , and the high-order one L_{sym} have been extensively studied and significant progress has been made over the past few

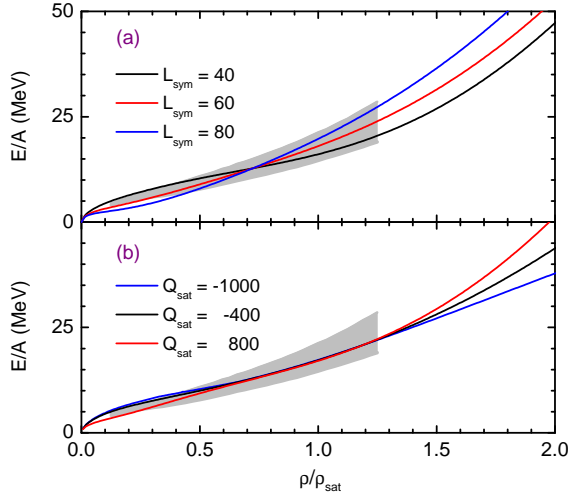


FIG. 1. Examples illustrating constraints on L_{sym} and Q_{sat} set by χEFT . Shown are the energy per particle of neutron matter as a function of ρ/ρ_{sat} for different values of L_{sym} [MeV] (a) and Q_{sat} [MeV] (b). The shaded bands show the χEFT results [44]. In each panel, only the indicated parameter is varied, whereas the remaining parameters are fixed at the default values.

decades. In particular, these parameters can be computed from any given energy density functional, therefore there is certain correlation between the input in the density functionals and these characteristics. This correlation suggests that one can generate a set of models by varying *only one* characteristic while fixing the others at saturation density. Note that the full set of these characteristics includes the five expansion coefficients in Eq. (9) plus the values of ρ_{sat} and M_D^* at saturation. We then further restrict the set of EoS by choosing only those which reproduce the result for neutron matter at densities below and around saturation derived from the *ab initio* calculations based on χEFT for densities up to $\sim 1.3\rho_{\text{sat}}$ [44].

While we fix the characteristics at saturation, the nuclei are most sensitive to the physics at densities that are below the saturation density. Indeed, it has been recognized by several authors [46, 79] that a variety of nuclear models which fit the properties of nuclear systems predict almost identical values of symmetry energy for the density $\rho_c = 0.11 \text{ fm}^{-3}$. Motivated by this, we hold the value of the symmetry energy $E_{\text{sym}}(\rho_c)$ [instead of $E_{\text{sym}}(\rho_{\text{sat}})$] constant when L_{sym} is being varied.

In Fig. 1 we show the EoS which are compatible with the neutron matter EoS and which lie within the allowed band region obtained from studies based on χEFT . These EoS are obtained by changing L_{sym} (upper panel) or Q_{sat} (lower panel), while keeping all other characteristics at their default values of DD-ME2 parametrization. It is seen that the uncertainties in the values of these parameters have minor influence on the behavior of the EoS at subsaturation density. However, they significantly affect the behavior of the EoS at higher density (above $\sim 2\rho_{\text{sat}}$). The energy of neutron matter below ρ_c (ρ_{sat}) becomes larger for the model with larger L_{sym} (Q_{sat}).

We also illustrate in Fig. 1 some typical cases for the neutron matter EoS that are outside the χEFT band. For $L_{\text{sym}} =$

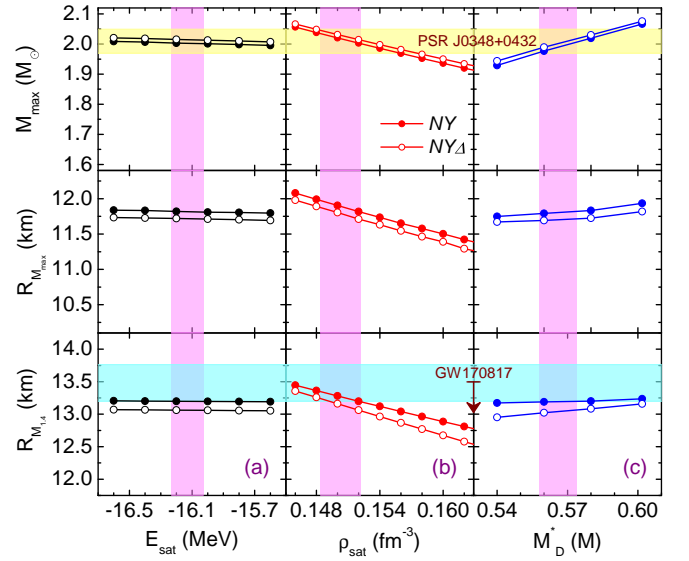


FIG. 2. Astrophysical characteristics of compact stars for nucleon–hyperon (NY) and nucleon–hyperon–Delta-resonance (NY Δ) compositions. The maximum mass M_{max} (upper panels), the corresponding radii $R_{M_{\text{max}}}$ (middle panels), and the radii $R_{M_{1.4}}$ for the canonical mass stars (lower panels) are varied by tuning individually the order-0 characteristics of nuclear matter at saturation point: the energy E_{sat} (a), the density ρ_{sat} (b), and the Dirac mass M_D^* (c), with the remaining parameters being fixed. The vertical shading in each figure indicates the effect of varying the values of parameters around their mean value considering 1σ deviation. The yellow shadings show the mass of PSR J0348+0432 [2]. The light-blue shadings indicate the spreads of the upper limit on the radius for a canonical $1.4M_{\odot}$ mass neutron star set by recent analysis of the tidal deformability determined from the GW170817 event [5–10].

80 MeV, it results in considerable deviation from χEFT calculations in the very low-density regime, although this value is still consistent with the bounds $L_{\text{sym}} = 58.7 \pm 28.1 \text{ MeV}$ obtained from the combined analysis of astrophysical constraints and terrestrial experiments [80]. As seen in Fig. 1, the energy is slightly overestimated compared to the χEFT calculations for $Q_{\text{sat}} = -1000 \text{ MeV}$ in the very low-density regime. This shows that the influence of Q_{sat} on the behavior of the EoS at subsaturation density is vanishing for $Q_{\text{sat}} \lesssim -500$. In the following, we shall restrict our attention to those EoS which satisfy the constraints on low-density neutron matter from χEFT calculations [44].

B. Uncertainties in characteristics and compact stars

We now assess the correlation between the gross properties of compact stars and each nuclear characteristics at saturation density. We base our exploration on the DD-ME2 interaction by varying individually the seven characteristics within their empirical uncertainty ranges. (Recall that we vary one characteristic at a time, i.e., all others are held fixed at their default values defined by the DD-ME2 parametrization). It is worthwhile to point out that although the five macroscopic charac-

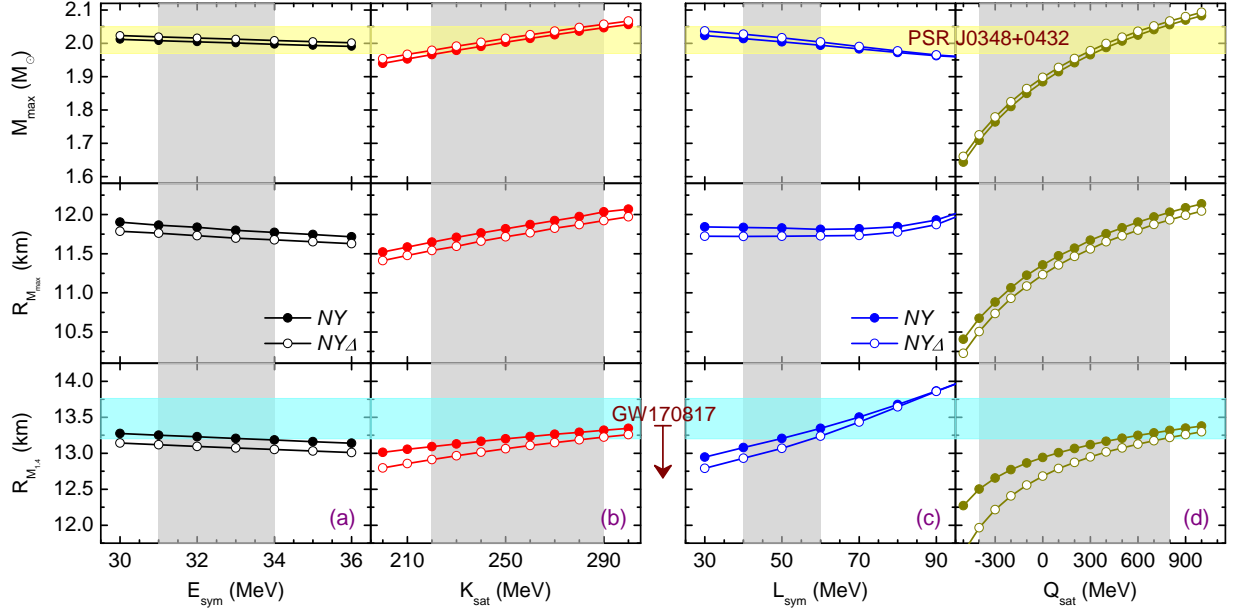


FIG. 3. Same as in Fig. 2, but for order-1 and -2 characteristics. The panels show the results of tuning of (a) symmetry energy E_{sym} , (b) compression modulus K_{sat} (c) slope of symmetry energy L_{sym} and (d) isoscalar skewness coefficient Q_{sat} . The vertical shading in each figure indicates the constraints from χ EFT calculations.

teristics listed in Eq. (9) together with ρ_{sat} and M_D^* coherently act on the EoS of dense matter, they are treated as independent of each other in the present analysis.

Figures 2 and 3 show the astrophysical characteristics of compact stars with hyperon (NY) and Delta resonance (NY Δ) compositions. We vary individually the characteristics at the order-0: E_{sat} , ρ_{sat} , and M_D^* , at the order-1: E_{sym} , K_{sat} , and at the order-2: L_{sym} , Q_{sat} . For illustrative purposes we fix the meson- Δ couplings assuming that the Δ potential satisfies the condition $V_{\Delta}(\rho_{\text{sat}}) = V_N(\rho_{\text{sat}})$. It should be mentioned that one has to modify all the 5 parameters in isoscalar sector in order to vary the order-0 characteristics, while one needs to modify only the 3 density-dependent parameters instead to vary the order-1 and 2 characteristics. In this context, variations of the order-1 and 2 characteristics do not impact the meson-hyperon and meson- Δ couplings at nuclear saturation density.

If hyperons and no Δ 's are admitted in stellar matter, the first hyperon to appear is the Λ , which is followed by the Ξ^- hyperon. The Σ hyperons are disfavored due to their repulsive potential at nuclear saturation density. This sequence of hyperon thresholds is consistent with the recent relativistic hypernuclear computations of Refs. [18, 60, 66]. As a result, the hyperons appear in compact stars with masses with $M_{\text{max}} \gtrsim 1.5M_{\odot}$, i.e., masses larger than the canonical pulsar mass. When Δ isobars are taken into account by taking $V_{\Delta}(\rho_{\text{sat}}) = V_N(\rho_{\text{sat}})$, Δ^- is the first isobar to be populated around $2\rho_{\text{sat}}$; its number density grows and reaches the number density of protons at $\sim 3\rho_{\text{sat}}$. At even higher densities it is gradually replaced by the Ξ^- hyperons around $4\rho_{\text{sat}}$. It has been shown that Δ -isobars soften the EoS at low densities but stiffen it at high densities [27]. (The corresponding

particle content of matter will be discussed below in Fig. 5.) It is thus seen that the overall trends are rather similar when varying individually the characteristics for NY and NY Δ matter. The difference between the two compositions is clearly reflected in the radius of a canonical neutron star. It is worthwhile to stress that in the entire parameter space considered, the purely nucleonic EoS models always predict a maximum mass of neutron star which is larger than $2M_{\odot}$.

It is seen from Fig. 2 that the maximum mass of a star M_{max} (the corresponding radius $R_{M_{\text{max}}}$) decreases with E_{sat} and ρ_{sat} , while it increases with M_D^* . The radius for a canonical star $R_{M_{1.4}}$ exhibits similar correlation. These features indicate that the gross properties of compact stars are sensitive to the values of ρ_{sat} and M_D^* . Since the parametrizations presented in Fig. 2 all satisfy the χ EFT constraint for neutron matter, we show instead the 1σ deviations that are evaluated from the available DD-RMF parameterizations. It is clearly seen that this model is well constrained with respect to the order-0 characteristics, within $\sim 2\%$. Therefore, the effect of varying the value of ρ_{sat} (or M_D^*) around the mean value at the level of 1σ deviation is not significant. It is worthwhile to mention that even the lowest order characteristics, for instance, the E_{sat} and ρ_{sat} could be different among different type of models, and the differences could be larger than the standard deviations. Indeed, while nonrelativistic models predict $\rho_{\text{sat}} \approx 0.160 \pm 0.004 \text{ fm}^{-3}$, the relativistic models have a significantly smaller value $\rho_{\text{sat}} \approx 0.150 \pm 0.003 \text{ fm}^{-3}$. In this context, the difference in the saturation density from relativistic and nonrelativistic models yields already considerable effects on gross properties of compact stars; see Fig. 2(b).

We now turn our attention to the assessment of the effects of higher order characteristics which are shown in Fig. 3. The

vertical shading indicates the constraints from χ EFT calculations. Besides this, we have checked that all the constrained parameter sets can reasonably reproduce the binding energies and charge radii of a number of (semi-)closed-shell nuclei with $\sim 2\%$ relative deviation. As seen from Fig. 3, the maximum mass M_{\max} is independent of the symmetry energy E_{sym} , while it shows a weak negative correlation with the slope parameter L_{sym} . The corresponding radius of the maximum-mass star $R_{M_{\max}}$ is essentially independent on the value of L_{sym} (and E_{sym}), while the radius of a canonical neutron star $R_{M_{1.4}}$ is strongly and almost linearly dependent on the value of L_{sym} . It is interesting to note that the key two astrophysical constraints available presently, i.e., $M_{\max} \gtrsim 2.0M_{\odot}$ and $R_{M_{1.4}} \lesssim 13.8$ km, favor small L_{sym} . As pointed out in Refs. [81, 82], there is a correlation between the radius of $1.4M_{\odot}$ stars and the magnitude of L_{sym} . However, once the constraints placed by χ EFT calculations are implemented, the isovector characteristics E_{sym} and L_{sym} have a very small influence on the gross properties of compact stars. For example, the variations in the maximum mass turn out to be of the order of $0.05 M_{\odot}$. The variations in the radius of a canonical neutron star are of the order of 0.4 km.

We further find that M_{\max} , $R_{M_{\max}}$ and $R_{M_{1.4}}$ display positive correlation with the isoscalar characteristics K_{sat} and Q_{sat} . The correlations are almost linear for K_{sat} but more complex for Q_{sat} . While isoscalar skewness Q_{sat} induces variation in both the maximum mass and radius, it largely controls the maximum mass of compact stars because it is most effective in modifying the EoS at supra-saturation densities. The seemingly stronger correlation between M_{\max} and Q_{sat} compared to the correlations of M_{\max} with the other six variables is because of the relatively larger uncertainty in Q_{sat} . In fact, the quality of resultant model depends not only on the form of the functional but, in addition, on the data used for its calibration. Indeed, even within the same functional form, the spread in values of Q_{sat} is very large, covering the range $\sim -500 < Q_{\text{sat}} < 500$ MeV [61, 77]. The constraint, $M_{\max} \gtrsim 2.0M_{\odot}$, favors larger values for Q_{sat} (or K_{sat}), but the constraint, $R_{M_{1.4}} \lesssim 13.8$ km, favors smaller values for Q_{sat} (or K_{sat}). Notice also the reduction of $R_{M_{1.4}}$ for negative values of Q_{sat} as seen in Fig. 3(d).

We now compare purely nucleonic compact stars with those which contain hyperonic matter. To support a purely nucleonic star with a mass of about $2.0M_{\odot}$, Q_{sat} needs to be just $Q_{\text{sat}} \gtrsim -650$ MeV, leading to a value of $R_{M_{1.4}}$ smaller than ~ 11.8 km. Once one allows for hyperonization, Q_{sat} has to be, at least, as large as ~ 300 MeV. Thus, once the value of the maximum mass of a compact star is pinned down, it will put a stringent upper limit on the Q_{sat} parameter. However, such a limit will largely depend on the composition of matter. It is interesting to notice that the maximum mass gradually saturates at the value $2.1M_{\odot}$ with an increase of the Q_{sat} . We conclude that our study indicates an upper limit $\sim 2.1M_{\odot}$ on the maximum mass of compact stars with hyperon mixing. This prediction will be further confirmed below, specifically in Fig. 6. Interestingly, the value we find is compatible with the most recent inferences on the maximum mass of neutron stars, $M_{\max} \sim 2.17M_{\odot}$ [83–85].

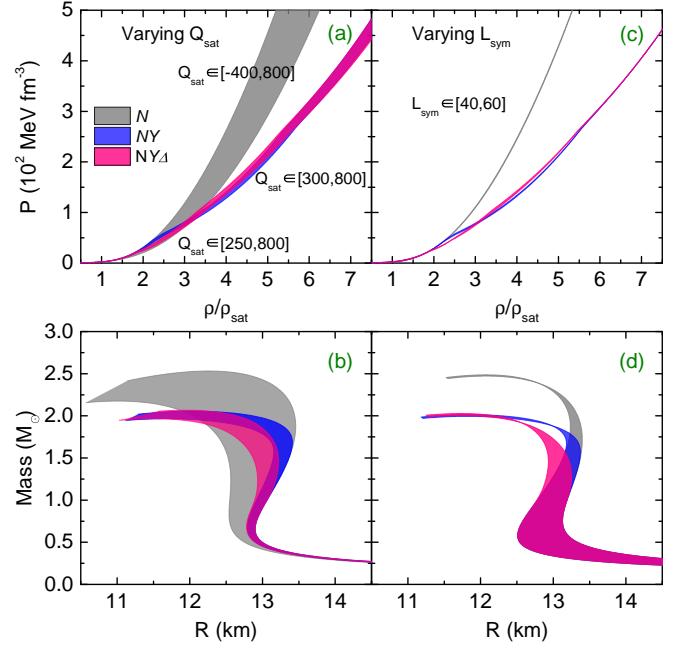


FIG. 4. EoS models and MR relations for N , NY , and $NY\Delta$ compositions of stellar matter. The bands are generated by varying the parameters Q_{sat} [MeV] (a, b) and L_{sym} [MeV] (c, d). The ranges of Q_{sat} and L_{sym} allowed by χ EFT and maximum mass constraints are indicated in the figures.

In Fig. 4 we show the EoS of stellar matter and the mass-radius (hereafter MR) relations for purely nucleonic, hyperon admixed and hyperon- Δ admixed matter for the allowed ranges of Q_{sat} (left panels) and L_{sym} (right panels). It is clearly seen that the same microscopical and astrophysical constraints lead to different EoS and MR relation depending on the assumed particle content. The appearance of hyperons and/or Δ -isobars softens the EoS from baryon density $\rho \sim 2.5\rho_{\text{sat}}$, which corresponds to the threshold of the Λ and/or Δ production. Furthermore, the displayed MR relations show that L_{sym} has appreciable effect on the radii of less massive stars ($M \leq 1.4M_{\odot}$), whereas the Q_{sat} has more significant effect on the radii of heavier stars ($M \geq 1.4M_{\odot}$). The canonical neutron stars are just at the intersection where the effects of Q_{sat} and L_{sym} on the radii is comparable, which implies that some combinations of Q_{sat} and L_{sym} can lead to the same $R_{M_{1.4}}$. Therefore, Q_{sat} or L_{sym} values alone are insufficient to characterize the low-density (up to around $2\rho_{\text{sat}}$) behavior of EoS. While one often uses the single parameter L_{sym} to characterize the predictions of different EoS models, such procedure is obviously not unambiguous.

Finally, we examine the effect of varying the value of Q_{sat} (upper panel) and L_{sym} (lower panel) on particle fraction which are shown in Fig. 5. By changing the value of Q_{sat} in the interval $[300, 800]$ MeV which corresponds to $\sim 50\%$ variations around its default value 480 MeV from DD-ME2, we observe that the effect of changing Q_{sat} on the onset density of Δ^- and Λ appears to be rather small, while its effect on the onset density of $\Xi^{-,0}$ is more visible. This is because Q_{sat}

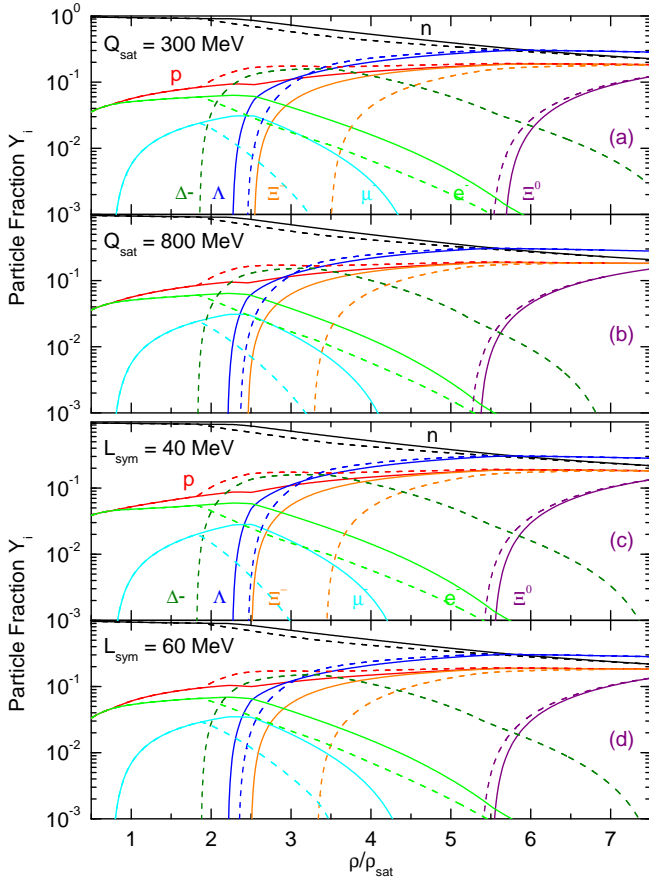


FIG. 5. Effect of varying the value of Q_{sat} [MeV] (a, b) and L_{sym} [MeV] (c, d) on particle fraction in NY (solid lines) NY Δ (dashed lines) stellar matter.

characterizes the medium- and high-density behavior of $E(\rho)$. As a result, the particle fractions shown in Fig. 5 (a) and (b) differ to some for $\rho \geq 3.5\rho_{\text{sat}}$. Varying the value of L_{sym} in the interval [40,60] MeV which corresponds to $\sim 20\%$ variations around its default DD-ME2 value ~ 50 MeV, we find that a larger value of L_{sym} pushes up the threshold density of Δ^- , while the onsets of Λ and Ξ^- are shifted down. Since the isovector field are largely suppressed at a higher density, the particle fractions shown in Fig. 5 (c) and (d) become identical for density $\gtrsim 5\rho_{\text{sat}}$.

In closing this section let us note the following. On one hand, the value of M_{max} for a compact star is basically determined by the isoscalar characteristics of the EoS, i.e., ρ_{sat} , K_{sat} , and Q_{sat} . The so-called “hyperon puzzle” [37] is therefore mainly related to the isoscalar skewness coefficient Q_{sat} that characterizes the medium- and high-density behavior of $E(\rho)$. On the other hand, the radius of the star is determined by both the isoscalar and isovector characteristics of the EoS. The constraints on neutron matter EoS coming from χEFT do not allow for a wide variation of L_{sym} , therefore one is left with the potential variations of Q_{sat} for the determination of the radius of a $1.4M_{\odot}$ star. Thus, we conclude that the observations of massive compact stars and advanced determinations of stellar radii will potentially constrain the value of Q_{sat} .

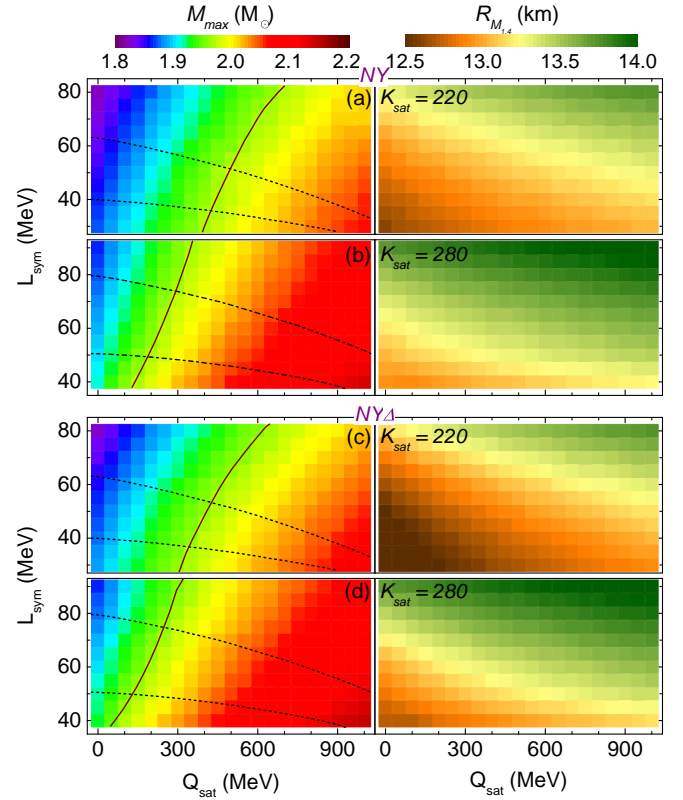


FIG. 6. Contour plots for the gross properties of compact stars in the parameter space spanned by L_{sym} and Q_{sat} (both in MeV) with two fixed values of $K_{\text{sat}} = 220$ and 280 MeV. Shown are the maximum mass and the radius of a canonical $1.4M_{\odot}$ mass star with NY (a, b) and NY Δ (c, d) compositions. The solid lines indicate the configurations that have a maximum mass equal to $1.97M_{\odot}$. The dashed lines show the constraints from χEFT calculations.

C. Observational constraints in the Q_{sat} - L_{sym} plane

Having established some general trends by varying only one of the parameters (i.e. only one of the dimensions in the parameter space) we would like to explore next the parameter space when two dimensions are varied. Our focus will be on the order-2 characteristics: Q_{sat} and L_{sym} which are less constrained so far. Fig. 6 shows the value of the maximum-mass star, and the radius of a canonical $1.4M_{\odot}$ star with NY and NY Δ compositions, computed by simultaneously varying both Q_{sat} and L_{sym} .

Comparing Fig. 6 (a) and (b), we observed that, (i) to satisfy the constraints imposed by χEFT , the value of L_{sym} has to be smaller for the EoS which has small K_{sat} , in order to enhance the contribution from the symmetry energy at very low density, see Fig. 1(a); (ii) to support compact stars with the maximum mass $M_{\text{max}} \gtrsim 1.97M_{\odot}$, the value of Q_{sat} has to be larger for the EoS which have small K_{sat} , to compensate the smaller contribution from the K_{sat} ; (iii) the maximum masses M_{max} (radii of $1.4M_{\odot}$ stars) predicted by EoS models with $K_{\text{sat}} = 220$ MeV are typically $\sim 0.1M_{\odot}$ (~ 0.3 km) smaller than those by EoSs with $K_{\text{sat}} = 280$ MeV; as already

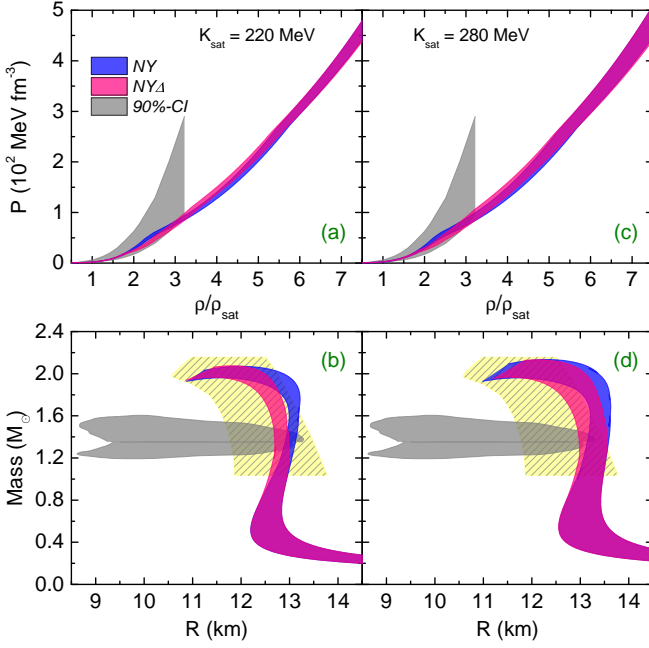


FIG. 7. EoS models and the corresponding MR relations for NY and $NY\Delta$ compositions and for $K_{\text{sat}} = 220$ MeV (a,b) and $K_{\text{sat}} = 280$ MeV (c, d) within the allowed parameter space spanned by Q_{sat} and L_{sym} (both in MeV). In the top panels, gray shading represents the 90% posterior credible level (90%CI) estimated from the binary neutron star merger event GW170817 [9]. In the bottom panels, gray shading represents the posterior for the mass and radius of each binary component using EoS-insensitive relations [9], while the yellow shading indicates the 2σ region of radii inferred in the analysis of Ref. [7].

observed in Fig. 3(b). As a consequence, the uncertainty in the incompressibility K_{sat} will impact the uncertainty interval of the skewness Q_{sat} , and vice versa.

Consider now the radius of a canonical $1.4M_{\odot}$ star with NY composition. For those EoS models that satisfy the χEFT and $M_{\text{max}} \gtrsim 2M_{\odot}$ constraints, the predicted radius of a $1.4M_{\odot}$ star spans from 12.8 km (defined by the EoS with $K_{\text{sat}} = 220$, $L_{\text{sym}} \approx 35$, $Q_{\text{sat}} \approx 450$ MeV) to 13.6 km (defined by the EoS with $K_{\text{sat}} = 280$, $L_{\text{sym}} \approx 60$, $Q_{\text{sat}} \approx 800$ MeV). Notice that the values $K_{\text{sat}} = 220$ MeV and $L_{\text{sym}} \approx 35$ MeV adopted here are already very close to the current lower bound of constraints on them placed by the combined analysis of terrestrial experiments [80, 86]. Therefore, the parameter space left for further reduction of the radius of a $1.4M_{\odot}$ star appears to be rather small.

When the Δ isobars are taken into account and one sets $V_{\Delta}(\rho_{\text{sat}}) = V_N(\rho_{\text{sat}})$ the magnitude of Q_{sat} may be taken to be slightly smaller (~ 50 MeV), than in the case of NY matter in order to obtain a $2M_{\odot}$ star. Indeed the inclusion of Δ resonances results in a larger maximum mass [27].

In Fig. 7 we summarize the EoS models (upper panels) and the corresponding MR relations (lower panels) for NY and $NY\Delta$ compositions with $K_{\text{sat}} = 220$ MeV (left panels) and $K_{\text{sat}} = 280$ MeV (right panels) respectively, restricting the $(Q_{\text{sat}}, L_{\text{sym}})$ space to that shown in Fig. 6. We also show the

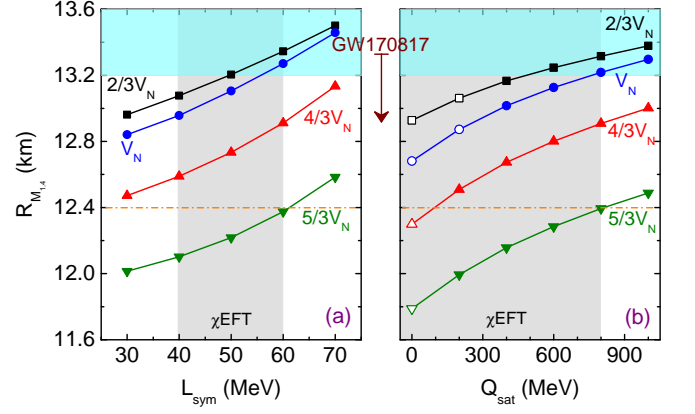


FIG. 8. Radii of canonical mass stars $R_{M,1.4}$ versus (a) the slope of symmetry energy L_{sym} and (b) the isoscalar skewness coefficient Q_{sat} at saturation density. The open symbols mark the cases where the maximum-mass is below $1.97M_{\odot}$. The vertical shadings indicate the constraints from χEFT calculations [44]. The light-blue shadings show the spreads of the upper limit for canonical $1.4M_{\odot}$ neutron stars set by recent analysis of the tidal deformability determined by GW170817 event [5–10]. The dashed lines mark the most likely value of 12.4 km set in Ref. [7].

constraints on the EoS obtained at the 90% posterior credible level (90%CI) from the binary neutron star merger event GW170817 [9], the posterior for the mass and radius of each binary component using EoS-insensitive relations in Ref. [9], as well as the probable (2σ region) radii of neutron stars estimated from a very large range of hadronic EoS by imposing constraints on the maximum mass and the tidal deformability [7]. Since the exotic degrees of freedom were not considered in Ref. [9], the band corresponding to 90%CI constraints on the high-density regime are not shown here. As can be seen from Fig. 7 (a) and (c), for the low-density region $0.5 \leq \rho/\rho_{\text{sat}} \leq 3$, our collection of EoS are fully consistent with the inference of Ref. [9]. The radii predicted by those models for a star with the canonical mass $1.4M_{\odot}$ lie close to the upper range of radii inferred from the analysis of tidal deformability from the binary neutron star inspiral event GW170817 [7, 9]. Those MR diagrams generated by EoS models which have $K_{\text{sat}} = 220$ MeV appear to be in better agreement with the 2σ domain inferred in Ref. [7].

Finally, it is worthwhile to note that if the vector meson-hyperon couplings are drawn from within the SU(3) flavor symmetric model [18, 60], rather than SU(6) spin-flavor symmetric model, then one can obtain stiffer equation of state at high densities (and less hyperon-rich matter) which would increase the maximum mass by about $0.3M_{\odot}$. In this case the value of Q_{sat} can be reduced by several hundreds without violating the astrophysical mass constraint.

D. Canonical mass stars with small radii

As mentioned in the previous section, the constraints on the tidal deformability have allowed for the determination of the statistically most probable radius of a $1.4M_{\odot}$ neutron

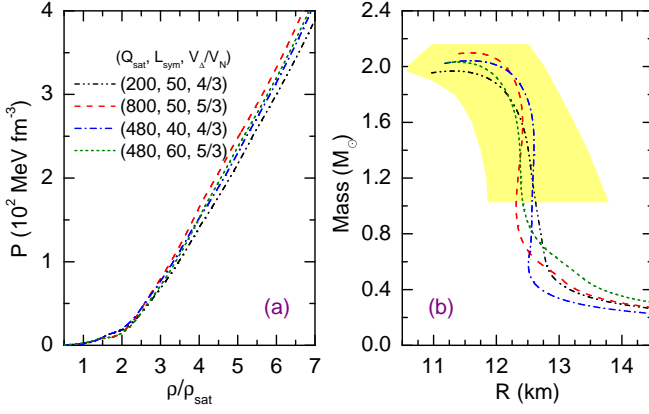


FIG. 9. EoS models and the corresponding MR relations for $NY\Delta$ stellar matter in the parameter space $(Q_{\text{sat}}, L_{\text{sym}}, V_{\Delta})$ (in MeV) that support a $1.4M_{\odot}$ neutron star with radius about 12.5 km. The yellow shading represents the probable (2σ region) radii of neutron stars estimated in Ref. [7].

stars. For instance, by imposing constraints on the maximum mass and on the dimensionless tidal deformability, it has been shown that a purely hadronic neutron star has $12.0 \leq R_{M_{1.4}} \leq 13.5$ km with a 2σ confidence level, with a most likely value of 12.4 km [7]. In Ref. [8] the binary neutron star mergers with different prior choices of masses have been analysed. Using Bayesian parameter estimation the authors concluded that the radius range is $8.9 \leq R_{M_{1.4}} \leq 13.2$ km, with an average value of $R = 10.8$ km [8].

The possibility that hyperonic stars have small radii in the range above is as exciting as it is challenging for nuclear theory. Notice that small radii demand a sufficiently soft EoS below $2-3\rho_{\text{sat}}$, while the observed large masses require that the same EoS must be able to evolve into a stiff EoS at high densities. In Ref. [27], it was augured that Δ isobars soften the EoS at low densities but stiffen it at high densities, resulting in significantly reduced radii and larger maximum masses of compact stars. The Δ isobars are therefore an interesting degree of freedom for the modeling of small-radius stars. The effects of Δ isobars have been illustrated for the case of $V_{\Delta} = V_N$ in previous sections. We next explore further their effect by varying the Δ -potential.

Figure 8 shows the radius for a $1.4M_{\odot}$ star as a function of L_{sym} (Q_{sat}) and V_{Δ} , while the remaining characteristic parameters are set as default values in Table I. As expected, the changes in the Δ -potential V_{Δ} have a stronger effect on the radius. The appearance of Δ isobars reduces the radius of a canonical star by up to 1 km for a reasonably attractive Δ -potential $V_{\Delta} = 5/3V_N$, thus producing a radius which is closer to the inferred most likely value 12.4 km obtained by Ref. [7]. It is worth noticing that the reduction is not sensitive to the values of Q_{sat} and/or L_{sym} .

We present in Fig. 9 several EoS models and the corresponding MR relations for $NY\Delta$ matter in the parameter space $(Q_{\text{sat}}, L_{\text{sym}}, V_{\Delta})$ that reproduce a $1.4M_{\odot}$ neutron star with a radius about 12.5 km. The particle fractions for two EoS models are shown in Fig. 10 for illustration. As can be seen in such

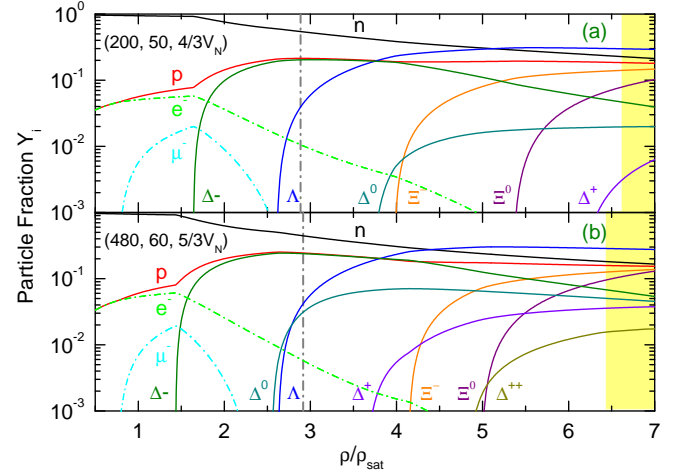


FIG. 10. Particle fraction for $NY\Delta$ stellar matter in the parameter space $(Q_{\text{sat}}, L_{\text{sym}}, V_{\Delta})$ (in MeV) that support a $1.4M_{\odot}$ neutron star with radius about 12.5 km. The thick vertical lines indicate the central density of the respective canonical $1.4M_{\odot}$ neutron star, the yellow shadings show densities beyond the maximum mass configurations.

configuration the Δ^- appears already at $\sim 1.5\rho_{\text{sat}}$, and Δ^0 appears at an intermediate densities. At the very central part of a canonical neutron star, the concentration of Δ^- isobars is close to that of protons.

Finally, in Fig. 11 we show the limits on the radius of a $1.4M_{\odot}$ canonical neutron star from the work which used the data on GW170817 event, along with the radii obtained from our EoS models assuming purely nucleonic (N), hyperon admixed (NY), and hyperon- Δ admixed ($NY\Delta$) particle composition. We recall that our limits are set on the $(K_{\text{sat}}, Q_{\text{sat}}, L_{\text{sym}})$ parameter space, by restricting $K_{\text{sat}} \in [220, 280]$. The value of the Δ -potential V_{Δ} is varied from $2/3V_N$ to $5/3V_N$. Further reduction of the radius up to 2 km can be obtained if one

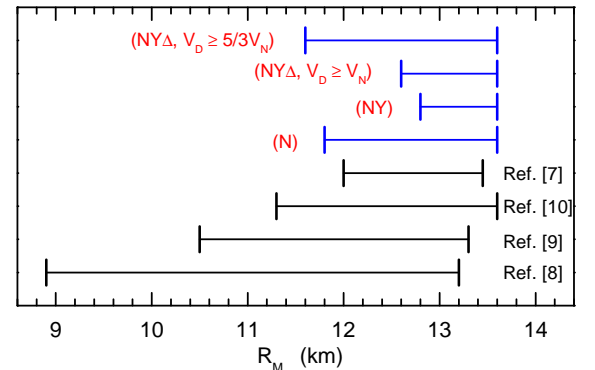


FIG. 11. Constraints on the radii of canonical neutron stars from the analysis of the GW170817 event using hadronic EoS models [7–10] and from present models assuming purely nucleonic (N), hyperon admixed (NY), and hyperon- Δ admixed ($NY\Delta$) particle composition for stellar matter. The limits are set on the parameter space spanned by $(K_{\text{sat}}, Q_{\text{sat}}, L_{\text{sym}})$ restricting K_{sat} within the range $[220, 280]$. The value of the Δ -potential is taken either $V_{\Delta} \geq V_N$ or $V_{\Delta} \geq 5/3V_N$.

further decrease the V_Δ , see Ref. [27] for a detailed discussion. It is clearly seen from Fig. 11 that our estimate of the upper limit of $R_{M_{1.4}}$ is consistent with other analyses [7–10]. The upper limit is in fact set by the purely nucleonic EoS, whereas the lower limit essentially depends on the assumed particle composition. Our hyperon- Δ admixed EoS models ($V_\Delta \geq 5/3V_N$) place a lower limit about 11.6 km. Interestingly, this limit is rather close to the one set by the purely nucleonic EoS model. It seems that $R_{M_{1.4}} \lesssim 11$ km is very marginally compatible with our present knowledge of the nuclear, hypernuclear and Δ resonance physics data. Canonical mass stars with small radii (less than 11 km) may therefore indicate the possibility of hadron-quark phase transition at density around $2\rho_{\text{sat}}$ [5, 7, 10, 11, 33].

IV. SUMMARY

Using the EoS for hadronic matter satisfying the latest constraints from both terrestrial nuclear experiments and astrophysical observations at saturation, as well as χ EFT of low-density neutron matter, we found that the gross properties of compact stars are very sensitive to the higher-order empirical parameters of nuclear matter around the saturation density, specifically the isoscalar skewness Q_{sat} and isovector slope L_{sym} . These are not well constrained from experiment, while

L_{sym} is constrained somewhat by χ EFT.

We observe that the Q_{sat} is the dominant parameter controlling both the maximum mass and the radius of a compact star. This is due to the fact that, on the one hand, the isovector characteristics E_{sym} and L_{sym} in Eq. (9) weakly influence the maximum mass, on the other hand, the strong restriction on the allowed values of L_{sym} coming from χ EFT does not allow for noticeable variations in the radius.

Another important point is that the upper limit on Q_{sat} is essentially dependent on the assumed particle composition of stellar matter. Our exploration of the parameter space shows that hyperonic stars more massive than $2M_\odot$ would require $Q_{\text{sat}} \geq 200$ MeV, leading to a radius $R_{M_{1.4}} \geq 12.8$ km. Including in the composition in addition the Δ isobars reduces the radius of a canonical mass star by about 1 km for a reasonably attractive Δ -potential, in agreement with previous findings [27, 69].

ACKNOWLEDGEMENTS

J. L. acknowledges the support by the Alexander von Humboldt foundation. A.S. acknowledges the support by the DFG (Grant No. SE 1836/4-1). Partial support was provided by the European COST Action “PHAROS” (CA16214) and the State of Hesse LOEWE-Program in HIC for FAIR.

-
- [1] P. B. Demorest, T. Pennucci, S. M. Ransom, M. S. E. Roberts, and J. W. T. Hessels, *Nature* **467**, 1081 (2010).
 - [2] J. Antoniadis, P. C. C. Freire, N. Wex, T. M. Tauris, R. S. Lynch, et al., *Science* **340**, 6131 (2013).
 - [3] E. Fonseca, T. T. Pennucci, J. A. Ellis, I. H. Stairs, D. J. Nice, et al., *Astrophys. J.* **832**, 167 (2016).
 - [4] B. P. Abbott, R. Abbott, T. D. Abbott, F. Acernese, K. Ackley, et al. (LIGO Scientific Collaboration and Virgo Collaboration), *Phys. Rev. Lett.* **119**, 161101 (2017).
 - [5] E. Annala, T. Gorda, A. Kurkela, and A. Vuorinen, *Phys. Rev. Lett.* **120**, 172703 (2018).
 - [6] F. J. Fattoyev, J. Piekarewicz, and C. J. Horowitz, *Phys. Rev. Lett.* **120**, 172702 (2018).
 - [7] E. R. Most, L. R. Weih, L. Rezzolla, and J. Schaffner-Bielich, *Phys. Rev. Lett.* **120**, 261103 (2018).
 - [8] S. De, D. Finstad, J. M. Lattimer, D. A. Brown, E. Berger, and C. M. Biwer, *Phys. Rev. Lett.* **121**, 091102 (2018).
 - [9] B. P. Abbott, R. Abbott, T. D. Abbott, F. Acernese, K. Ackley, et al. (The LIGO Scientific Collaboration and the Virgo Collaboration), *Phys. Rev. Lett.* **121**, 161101 (2018).
 - [10] I. Tews, J. Margueron, and S. Reddy, *Phys. Rev. C* **98**, 045804 (2018).
 - [11] V. Paschalidis, K. Yagi, D. Alvarez-Castillo, D. B. Blaschke, and A. Sedrakian, *Phys. Rev. D* **97**, 084038 (2018).
 - [12] N. K. Glendenning, *Astrophys. J.* **293**, 470 (1985).
 - [13] N. K. Glendenning and S. A. Moszkowski, *Phys. Rev. Lett.* **67**, 2414 (1991).
 - [14] J. Schaffner, C. B. Dover, A. Gal, C. Greiner, D. J. Millener, and H. Stocker, *Ann. Phys.* **235**, 35 (1994).
 - [15] H. Huber, F. Weber, M. K. Weigel, and C. Schaab, *Int. J. Mod. Phys. E* **7**, 301 (1998).
 - [16] I. Vidaña, A. Polls, A. Ramos, and H.-J. Schulze, *Phys. Rev. C* **64**, 044301 (2001).
 - [17] S. Weissenborn, D. Chatterjee, and J. Schaffner-Bielich, *Nucl. Phys. A* **881**, 62 (2012).
 - [18] S. Weissenborn, D. Chatterjee, and J. Schaffner-Bielich, *Phys. Rev. C* **85**, 065802 (2012).
 - [19] G. Colucci and A. Sedrakian, *Phys. Rev. C* **87**, 055806 (2013).
 - [20] E. van Dalen, G. Colucci, and A. Sedrakian, *Phys. Lett. B* **734**, 383 (2014).
 - [21] M. Oertel, C. Providência, F. Gulminelli, and A. R. Raduta, *J. Phys. G* **42**, 075202 (2015).
 - [22] L. Tolos, M. Centelles, and A. Ramos, *Astrophys. J.* **834**, 3 (2016).
 - [23] A. R. Raduta, A. Sedrakian, and F. Weber, *Mon. Not. R. Astron. Soc.* **475**, 4347 (2017).
 - [24] M. Prakash, M. Prakash, J. M. Lattimer, and C. J. Pethick, *Astrophys. J.* **390**, L77 (1992).
 - [25] T. Schürhoff, S. Schramm, and V. Dexheimer, *Astrophys. J.* **724**, L74 (2010).
 - [26] A. Drago, A. Lavagno, and G. Pagliara, *Phys. Rev. D* **89**, 043014 (2014).
 - [27] J. J. Li, A. Sedrakian, and F. Weber, *Phys. Lett. B* **783**, 234 (2018).
 - [28] P. Haensel, J. L. Zdunik, and R. Schaefer, *Astron. astrophys.* **160**, 121 (1986).
 - [29] H. Heiselberg, C. J. Pethick, and E. F. Staubo, *Phys. Rev. Lett.* **70**, 1355 (1993).
 - [30] F. Weber, *Prog. Part. Nucl. Phys.* **54**, 193 (2005).
 - [31] L. Bonanno and A. Sedrakian, *Astron. Astrophys.* **539**, A16 (2012).

- [32] M. G. Alford, S. Han, and M. Prakash, *Phys. Rev. D* **88**, 083013 (2013).
- [33] M. Alford and A. Sedrakian, *Phys. Rev. Lett.* **119**, 161104 (2017).
- [34] D. Alvarez-Castillo, S. Benic, D. Blaschke, S. Han, and S. Typel, *Eur. Phys. J. A* **52**, 232 (2016).
- [35] D. E. Alvarez-Castillo and D. B. Blaschke, *Phys. Rev. C* **96**, 045809 (2017).
- [36] K. Yagi and N. Yunes, *Phys. Rep.* **681**, 1 (2017).
- [37] D. Chatterjee and I. Vidaña, *Eur. Phys. J. A* **52**, 29 (2016).
- [38] A. Sedrakian, in *EPJ Web Conf.* (EDP Sciences, 2017), vol. 164, p. 01009.
- [39] G. Baym, T. Hatsuda, T. Kojo, P. D. Powell, Y. Song, and T. Takatsuka, *Rep. Prog. Phys.* **81**, 056902 (2018).
- [40] A. W. Steiner, J. M. Lattimer, and E. F. Brown, *Astrophys. J.* **722**, 33 (2010).
- [41] A. W. Steiner, J. M. Lattimer, and E. F. Brown, *Astrophys. J. Lett.* **765**, L5 (2013).
- [42] J. M. Lattimer and A. W. Steiner, *Astrophys. J.* **784**, 123 (2014).
- [43] F. Özel, D. Psaltis, T. Güver, G. Baym, C. Heinke, and S. Guillot, *Astrophys. J.* **820**, 28 (2016).
- [44] C. Drischler, A. Carbone, K. Hebeler, and A. Schwenk, *Phys. Rev. C* **94**, 054307 (2016).
- [45] L.-W. Chen, C. M. Ko, B.-A. Li, and J. Xu, *Phys. Rev. C* **82**, 024321 (2010).
- [46] Z. Zhang and L.-W. Chen, *Phys. Lett. B* **726**, 234 (2013).
- [47] L.-W. Chen and J.-Z. Gu, *J. Phys. G: Nucl. Part. Phys.* **39**, 035104 (2012).
- [48] Z. Zhang and L.-W. Chen, *Phys. Rev. C* **90**, 064317 (2014).
- [49] B.-J. Cai, F. J. Fattoyev, B.-A. Li, and W. G. Newton, *Phys. Rev. C* **92**, 015802 (2015).
- [50] B.-J. Cai and L.-W. Chen, *Nucl. Sci. Tech.* **28**, 185 (2017).
- [51] F. J. Fattoyev, J. Carvajal, W. G. Newton, and B.-A. Li, *Phys. Rev. C* **87**, 015806 (2013).
- [52] J. Margueron, R. Hoffmann Casali, and F. Gulminelli, *Phys. Rev. C* **97**, 025806 (2018).
- [53] N.-B. Zhang, B.-A. Li, and J. Xu, *Astrophys. J.* **859**, 90 (2018).
- [54] D. Vretenar, A. V. Afanasjev, G. A. Lalazissis, and P. Ring, *Phys. Rep.* **409**, 101 (2005).
- [55] J. Meng, H. Toki, S.-G. Zhou, S. Q. Zhang, W. H. Long, and L. S. Geng, *Prog. Part. Nucl. Phys.* **57**, 470 (2006).
- [56] B. D. Serot and J. D. Walecka, *Int. J. Mod. Phys. E* **6**, 515 (1997).
- [57] V. Pascalutsa, M. Vanderhaeghen, and S. N. Yang, *Phys. Rep.* **437**, 125 (2007).
- [58] X. Roca-Maza, X. Viñas, M. Centelles, P. Ring, and P. Schuck, *Phys. Rev. C* **84**, 054309 (2011).
- [59] W.-H. Long, N. Van Giai, and J. Meng, *Phys. Lett. B* **640**, 150 (2006).
- [60] J. J. Li, W. H. Long, and A. Sedrakian, *Eur. Phys. J. A* **54**, 133 (2018).
- [61] S. Typel and H. H. Wolter, *Nucl. Phys. A* **656**, 331 (1999).
- [62] T. Nikšić, D. Vretenar, P. Finelli, and P. Ring, *Phys. Rev. C* **66**, 024306 (2002).
- [63] A. Feliciello and T. Nagae, *Rep. Prog. Phys.* **78**, 096301 (2015).
- [64] A. Gal, E. V. Hungerford, and D. J. Millener, *Rev. Mod. Phys.* **88**, 035004 (2016).
- [65] J. K. Ahn, H. Akikawa, S. Aoki, K. Arai, S. Y. Bahk, et al. (E373 (KEK-PS) Collaboration), *Phys. Rev. C* **88**, 014003 (2013).
- [66] M. Fortin, S. S. Avancini, C. Providência, and I. Vidaña, *Phys. Rev. C* **95**, 065803 (2017).
- [67] W. M. Alberico, G. Gervino, and A. Lavagno, *Phys. Lett. B* **321**, 177 (1994).
- [68] S. X. Nakamura, T. Sato, T.-S. H. Lee, B. Szczerbinska, and K. Kubodera, *Phys. Rev. C* **81**, 035502 (2010).
- [69] A. Drago, A. Lavagno, G. Pagliara, and D. Pigato, *Phys. Rev. C* **90**, 065809 (2014).
- [70] G. Ferini, M. Colonna, T. Gaitanos, and M. Di Toro, *Nucl. Phys. A* **762**, 147 (2015).
- [71] M. D. Cozma, *Phys. Lett. B* **753**, 166 (2016).
- [72] E. E. Kolomeitsev, K. A. Maslov, and D. N. Voskresensky, *Nucl. Phys. A* **961**, 106 (2017).
- [73] G. Baym, C. Pethick, and P. Sutherland, *Astrophys. J.* **170**, 299 (1971).
- [74] G. Baym, H. A. Bethe, and C. J. Pethick, *Nucl. Phys. A* **175**, 225 (1971).
- [75] R. C. Tolman, *Phys. Rev.* **55**, 364 (1939).
- [76] J. R. Oppenheimer and G. M. Volkoff, *Phys. Rev.* **55**, 374 (1939).
- [77] G. A. Lalazissis, T. Nikšić, D. Vretenar, and P. Ring, *Phys. Rev. C* **71**, 024312 (2005).
- [78] J. Margueron, R. Hoffmann Casali, and F. Gulminelli, *Phys. Rev. C* **97**, 025805 (2018).
- [79] C. Ducoin, J. Margueron, C. Providência, and I. Vidaña, *Phys. Rev. C* **83**, 045810 (2011).
- [80] M. Oertel, M. Hempel, T. Klähn, and S. Typel, *Rev. Mod. Phys.* **89**, 015007 (2017).
- [81] C. J. Horowitz and J. Piekarewicz, *Phys. Rev. Lett.* **86**, 5647 (2001).
- [82] M. Fortin, C. Providência, A. R. Raduta, F. Gulminelli, J. L. Zdunik, P. Haensel, and M. Bejger, *Phys. Rev. C* **94**, 035804 (2016).
- [83] B. Margalit and B. D. Metzger, *Astrophys. J. Lett.* **850**, L19 (2017).
- [84] M. Shibata, S. Fujibayashi, K. Hotokezaka, K. Kiuchi, K. Kyutoku, Y. Sekiguchi, and M. Tanaka, *Phys. Rev. D* **96**, 123012 (2017).
- [85] L. Rezzolla, E. R. Most, and L. R. Weih, *Astrophys. J. Lett.* **852**, L25 (2018).
- [86] D. Vretenar, T. Nikšić, and P. Ring, *Phys. Rev. C* **68**, 024310 (2003).